Journal of ELECTRONIC MATERIALS, Vol. 40, No. 10, 2011
DOI: 10.1007/s11664-011-1707-9

Effects of Sm^{3+} Doping on Dielectric Properties of Anatase TiO_2 Nanoparticles Synthesized by a Low-Temperature Hydrothermal Method

A.K. ABDUL GAFOOR,[1] JESTY THOMAS,[2] M.M. MUSTHAFA,[1] and P.P. PRADYUMNAN[1,3]

1.—Department of Physics, University of Calicut, Malappuram 673635, Kerala, India. 2.—School of Chemical Sciences, Mahatma Gandhi University, Kottayam 686560, Kerala, India. 3.—e-mail: pradyupp@gmail.com

Samarium-doped thermally stable TiO_2 nanoparticles in the anatase phase have been synthesized by a low-temperature hydrothermal method. The formation of the anatase phase has been investigated by x-ray diffraction. Thermogravimetry and differential thermal analysis have been used for thermal studies. The morphology and composition of synthesized powders have been studied using scanning electron microscopy, transmission electron microscopy, and energy-dispersive spectroscopy. Surface areas were studied by the Brunauer–Emmett–Teller method. Dielectric properties were studied for dopant levels of 0.2 mol% and 0.5 mol% at 300 K in the frequency range of 42 Hz to 5 MHz. At low frequency, charge carriers at the grain boundary produce interfacial polarization giving rise to a high dielectric constant (ε'), which is significantly reduced by doping with samarium ions (Sm^{3+}). Strong frequency dependence of the dielectric loss was also observed for each concentration. Conductivity studies showed that the reduction in conductivity is due to the decrease in particle size with the increase in Sm^{3+} dopant level.

Key words: Samarium-doped TiO_2, nanoparticles, dielectric properties, conductivity

INTRODUCTION

Nanoscale semiconductors have attracted increasing interest due to their impact in catalytic, magnetic, optical, and electrical applications. These materials exhibit a variety of superior properties when compared with their bulk form. The size dependence of the properties of semiconductor nanoparticles is important and offers an opportunity to fabricate exotic new devices. Nanotitania (TiO_2) is one of the important ionic semiconductors with diverse application in photocatalysis, dye-sensitized solar cells, and as an anode material for lithium-ion batteries. It has been studied extensively by various groups.[1–5] Nanotitania, a cost-effective material which also has the advantages of high dielectric constant[6,7] and promising chemical stability,[8] is expected to replace traditional capacitor dielectrics and dielectric resonators. The majority of dielectric applications are affected by the presence of various crystalline polymorphs and morphologies;[9] dielectric properties are strongly influenced by the nature of polarization and are very sensitive to interfaces, grain scale, strain introduction, and doping by ions. One of the authors has already reported photocatalytic properties of nanotitania doped with samarium.[5] The present work aims to investigate how doping nanotitania with a rare-earth impurity such as samarium could change its dielectric and electrical properties.

Numerous synthetic methods such as the sol–gel method, chemical vapor deposition, the hydrothermal method, and pulsed laser deposition have been used for fabrication of anatase phase TiO_2 nano-

(Received November 8, 2010; accepted June 20, 2011; published online July 19, 2011)

particles.[10–16] A literature survey revealed that no systematic studies have been reported on the physical properties and device parameters of hydrothermally synthesized anatase phase TiO_2 and doped TiO_2 nanoparticles. In the present study, 0.2 mol% and 0.5 mol% Sm^{3+}-doped nanotitania materials were prepared using a low-temperature hydrothermal method. The influences of Sm^{3+} doping on the dielectric and electrical properties of TiO_2 nanoparticles were then studied. It was observed that the dielectric constant was high in the low-frequency region and stable above 10 kHz for all the synthesized samples. The loss tangent peak of TiO_2 was shifted from 1 kHz to 2 kHz upon doping, and the peak intensity was found to increase with dopant concentration. The dependence of the electrical conductivity of the sample on frequency was studied at room temperature. At room temperature, the alternating current (AC) conductivity was found to increase with the frequency of applied electric field according to the universal power law.[17] The effects on electrical conductivity of nanostructures and nanomaterials are complex, since they are based on distinctive mechanisms. In our study, the AC conductivity of TiO_2 was found to decrease with increasing samarium dopant concentration.

EXPERIMENTAL PROCEDURES

Analytical-grade titanium (IV) isopropoxide ($Ti[OC_3H_7]_4$) acquired from Acros Organics and $SmCl_3$ from Aldrich Chemicals Sigma (99.9% pure grade) were used for the synthesis. Deionized water was used throughout the experiments.

$SmCl_3$ (0.1 M) was added as dopant to 7.0 ml titanium (IV) isopropoxide, and the mixture was stirred vigorously; the mol% of samarium ion with respect to titanium was set to 0.2 mol% and 0.5 mol%. Distilled water was added until the white precipitate was completely formed. The pH of the mixture was maintained at 7.0 by addition of ammonia, and then it was transferred to a stainless-steel Teflon-lined autoclave, and hydrothermal reaction was allowed to proceed at 200°C for 2 h. The synthesized powders were filtered, washed with water and acetone, and then dried at 80°C.

Characterization and Measurements

X-ray diffraction patterns (XRD) of synthesized samples were recorded on a Bruker Advance diffractometer using Cu K_α radiation (λ = 0.15406 nm) at scanning rate of 0.02^0/s in the 2θ range of 10° to 80°. The Brunauer–Emmett–Teller (BET) specific surface area of the powder was measured using nitrogen adsorption and a surface area analyzer (Micromeritics, Gemini, USA). Thermogravimetry (TG) and differential thermal analysis (DTA) measurements were carried out using a Shimadzu DTG-60 device. Particle size, composition, and structure were also studied using scanning electron microscopy (SEM, Jeol, 6390 LA), energy-dispersive spectroscopy (EDS), and transmission electron microscopy (TEM, Jeol JEM-3010) at an accelerating voltage of 100 kV.

The nanopowders were consolidated in the form of cylindrical pellets of 11 mm diameter and 1 mm thickness by applying a force of about 8 ton for 3 min using a hydraulic press. Dielectric measurements were carried out at room temperature using an impedance analyzer by applying an AC signal across the sample cell with a blocking electrode (silver) in a dielectric cell connected to a computer-controlled HOIKI LCR Hi-Tester 3532-50 setup, in the frequency range of 42 Hz to 5 MHz. The real component of the complex dielectric function (ε'), the loss tangent (tan δ), and the AC conductivity (σ_{AC}) were calculated from the measured data using the dimensions of the pellets.

RESULTS AND DISCUSSION

X-Ray Diffraction Analysis

The crystalline phase of the prepared nanoparticles was analyzed by XRD, and the results are shown in Fig. 1. XRD patterns revealed that the samples had a high degree of crystallinity, and the observed peaks could be indexed to the anatase phase tetragonal structure of TiO_2 (JCPDS, no. 21-1272). No samarium oxide peaks were found in the XRD patterns, due to the low doping concentration. Figure 1 shows broader x-ray diffraction peaks for the samarium-doped TiO_2 samples due to the smaller grain size. Similarly, Mona et al. reported broadening of XRD peaks on lanthanide ion doping.[18]

The nanocrystallite sizes of the samples were estimated using the Debye–Scherrer equation, $D_{XRD} = 0.9\ \lambda/\beta\ \cos\theta$, where D is the crystallite size, λ is the wavelength of x-ray used, and β and θ are the full-width at half-maximum of the XRD diffraction

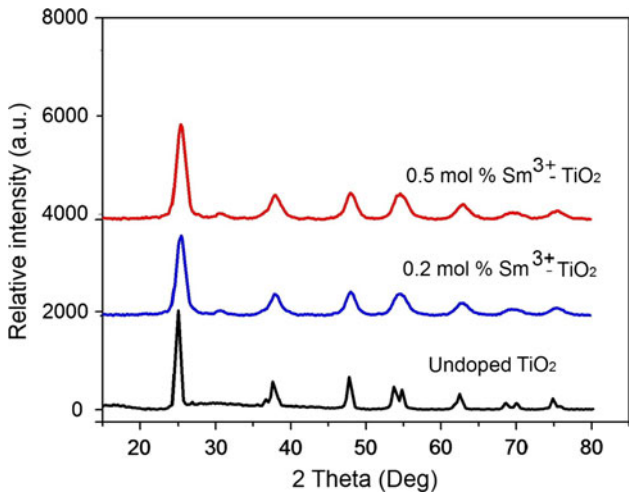

Fig. 1. X-ray diffraction patterns of undoped TiO_2, 0.2 mol% Sm^{3+}-TiO_2, and 0.5 mol% Sm^{3+}-TiO_2 nanoparticles.

Table I. Crystallite sizes, surface areas, and particle sizes of undoped TiO_2, 0.2 mol% Sm^{3+}-TiO_2, and 0.5 mol% Sm^{3+}-TiO_2 nanoparticles

Samples	Crystallite Size, D_{XRD} (nm)	Specific Surface Area (m^2/g)	Particle Size, D_{BET} (nm)
Undoped TiO_2	31	49.98	31
0.2 mol% Sm^{3+}-TiO_2	10	107.16	14
0.5 mol% Sm^{3+}-TiO_2	8	128.50	12

intensity lines and the half diffraction angle (2θ), respectively. Table I shows that the crystallite size of nanotitania decreased with samarium doping, which is in agreement with earlier reports.[19–21] The present study revealed that doping with samarium ions hindered the increase in grain size during hydrothermal synthesis.

Nanostructural Analysis

Nanostructural analysis using SEM and TEM supplemented by EDS was carried out for all the samples to establish the grain sizes and determine the chemical composition. Strong x-ray peaks associated with Ti K_α and Sm K_α were found in the EDS spectrum (Fig. 2a–c). Quantitative analysis by the EDS software package was used to determine the respective atomic percentages of each element in the sample. SEM micrographs of the undoped and Sm^{3+}-doped samples, displayed in Fig. 2, showed the agglomeration of the nanoparticles. The average grain diameter was measured as being in the range of a few nanometers. The TEM images (Fig. 3a–c), showed the uniform nature of particles with no change in particle morphology due to samarium doping. Also, samarium oxide particles were not identified in the TEM images, as they were well dispersed.

The specific surface area of the powders was measured by the dynamic BET method, in which N_2 gas was adsorbed at 77 K using a Micromeritics system. The surface areas measured for the Sm^{3+}-doped samples were higher than that for the undoped sample (Table 1). The high surface area was due to the reduction of the TiO_2 crystallite size brought about by the samarium ions. However, there was only a slightly higher surface area when the Sm^{3+} content was 0.5 mol% rather than 0.2 mol%. An increase in surface area on Nd^{3+} doping was reported by De et al.[22] The average particle sizes were calculated from the BET surface area using the equation $D_{BET} = 6000/\rho S$, where D_{BET} is the average nanoparticle size (nm), ρ is the powder density (g/cm^3), and S is the specific surface area (m^2/g). The results were comparable to the average nanocrystallite size obtained using Scherrer's equation and complemented the findings from the SEM and TEM micrographs. The TG-DTA data (at heating rate of 10°C/min) for the doped and undoped samples are shown in Figs. 4 and 5, respectively. It was clear from the data that the samples were thermally stable because there was no weight loss or phase transformation in the 30°C to 1000°C temperature range.

Permittivity and AC Conductivity

Dielectric measurements at room temperature were performed on undoped and Sm^{3+}-doped TiO_2 nanoparticles. Figure 6 shows the variation of loss tangent (tan δ) with frequency for doped and undoped samples. The loss spectra were characterized by peaks appearing at characteristic frequencies for both the undoped and doped samples, suggesting the existence of relaxing dipoles in all the samples. The strength and frequency of relaxation depend on the characteristic property of dipolar relaxation. The tangent loss peak for undoped TiO_2 was at 1 kHz. It shifted to a higher frequency, i.e., 2 kHz, on samarium doping, while the peak intensity was found to increase upon increasing the samarium dopant concentration. Dielectric relaxation observed for samples at low frequencies was due to the dominant effect of polarization due to charge migration. However, as the frequency increased, dielectric relaxation was found to be small, and above 100 kHz frequency-independent behavior was observed for all the samples. In normal dielectric behavior, the dielectric constant remains almost constant at high frequencies, because, beyond a certain frequency, intrawell hopping becomes prominent and charge carriers do not have sufficient time for long-range hopping before the field reversal takes place. As a result, in the high frequency range, only intrawell hopping persists, because the average hopping distance for intrawell hopping is one lattice spacing, while for interwell hopping, it is of the order of a few nanometers. So polarization decreases as the signal frequency is increased. The dielectric constant of all samples as a function of frequency at room temperature is shown in Fig. 7. The nature of dielectric permittivity related to free dipoles oscillating in an alternating field is as follows. At very low frequencies ($\omega \ll 1/\tau$), where τ is the relaxation time, dipoles follow the field and $\varepsilon' \approx \varepsilon_s$ (the dielectric constant at quasistatic field). As the frequency increases (with $\omega < 1/\tau$), dipoles begin to lag behind the field and ε' slightly decreases. When the frequency reaches the characteristic frequency

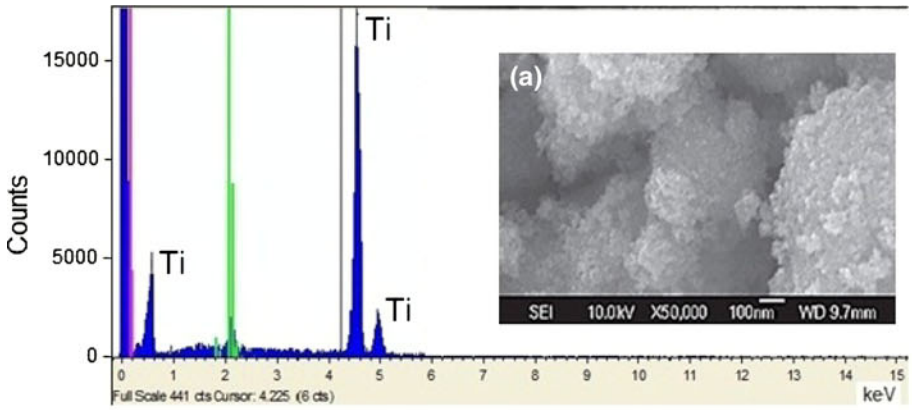

Element	Weight %	Weight % σ	Atomic %
Titanium	100.00	0.00	100.00

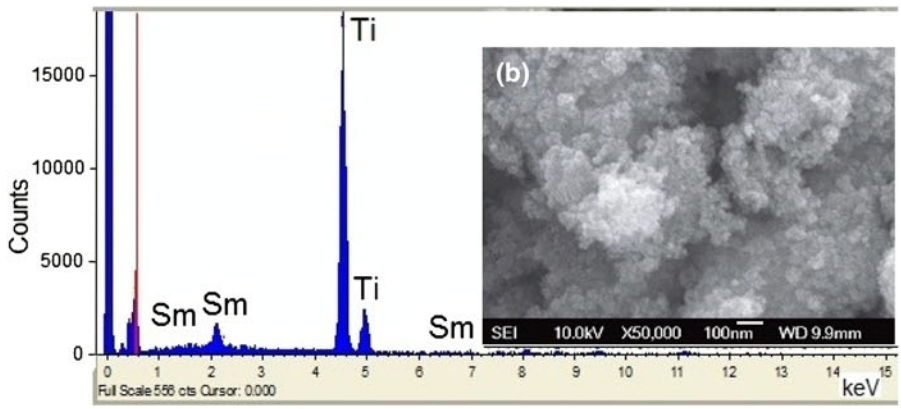

Element	Weight %	Weight % σ	Atomic %
Titanium	99.26	4.14	99.82
Samarium	0.74	4.14	0.18

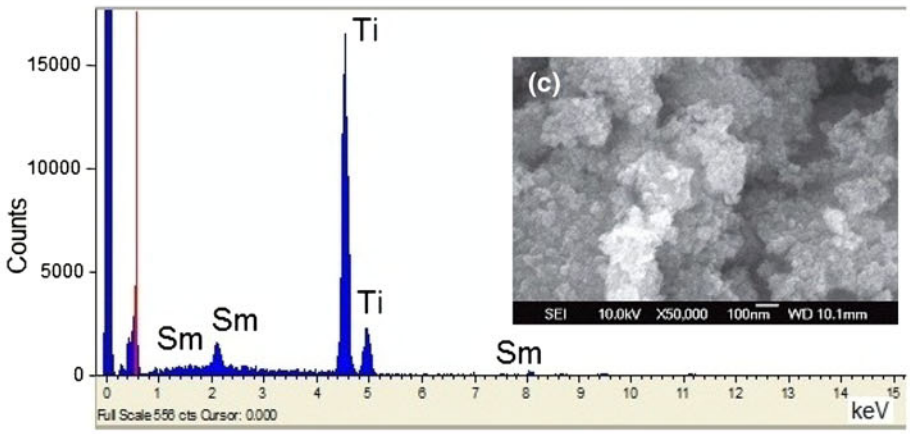

Element	Weight %	Weight % σ	Atomic %
Titanium	98.63	1.29	99.66
Samarium	1.37	1.29	0.34

Fig. 2. SEM and EDS images of (a) undoped TiO_2, (b) 0.2 mol% Sm^{3+}-TiO_2, and (c) 0.5 mol% Sm^{3+}-TiO_2.

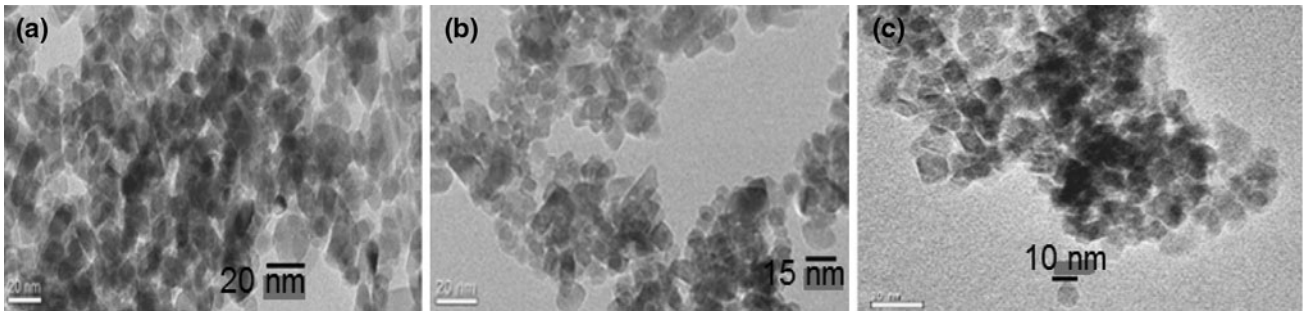

Fig. 3. TEM micrographs of (a) undoped TiO_2, (b) 0.2 mol% Sm^{3+}-TiO_2, and (c) 0.5 mol% Sm^{3+}-TiO_2.

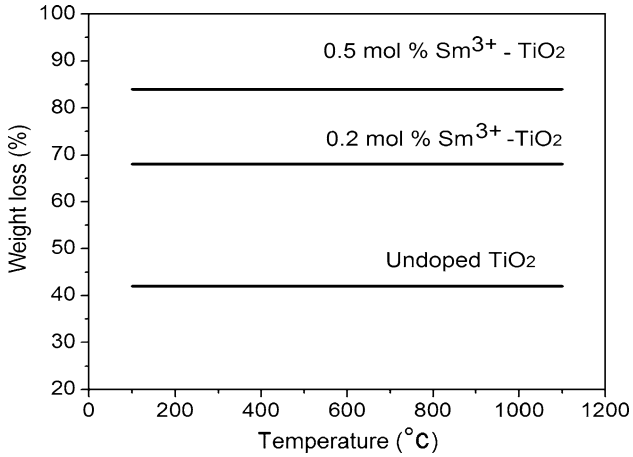

Fig. 4. TG curves of undoped TiO_2, 0.2 mol% Sm^{3+}-TiO_2, and 0.5 mol% Sm^{3+}-TiO_2 nanoparticles.

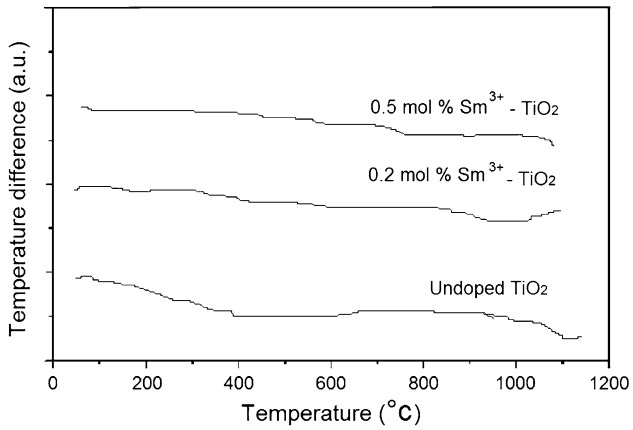

Fig. 5. DTA curves of undoped TiO_2, 0.2 mol% Sm^{3+}-TiO_2, and 0.5 mol% Sm^{3+}-TiO_2 nanoparticles.

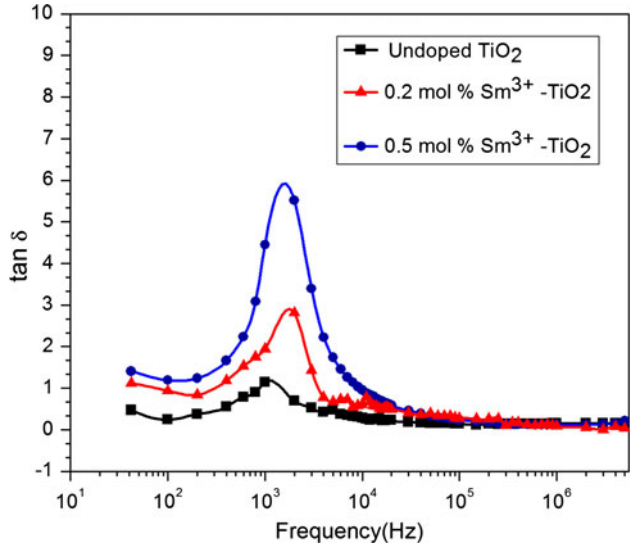

Fig. 6. Variation of dielectric loss with frequency of undoped TiO_2, 0.2 mol% Sm^{3+}-TiO_2, and 0.5 mol% Sm^{3+}-TiO_2 nanoparticles.

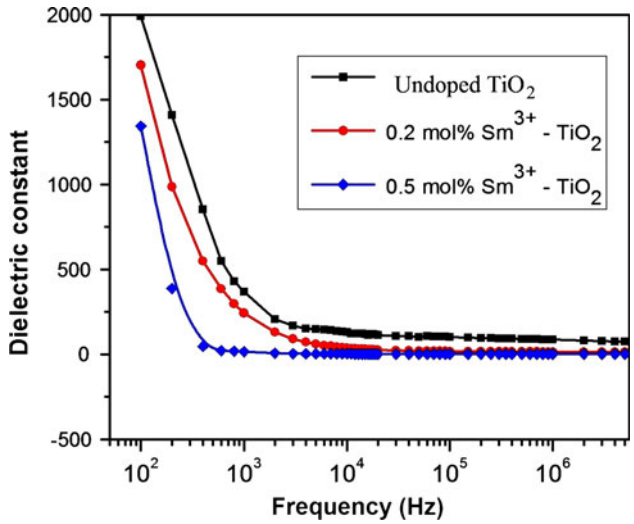

Fig. 7. Variation of dielectric constant of undoped TiO_2, 0.2 mol% Sm^{3+}-TiO_2, and 0.5 mol% Sm^{3+}-TiO_2 nanoparticles.

($\omega = 1/\tau$), the dielectric constant drops (relaxation process). At very high frequencies ($\omega \gg 1/\tau$), dipoles can no longer follow the field and $\varepsilon' = \varepsilon_\infty$ (high-frequency value of ε'). This behavior was observed for the doped and undoped TiO_2 samples. The higher values of ε' at lower frequency were due to the simultaneous presence of space charge, dipolar, ionic, and electronic polarizations. At room temperature, in the low frequency region, the dielectric constant of undoped TiO_2 decreased on doping with Sm because the 4*f* level of samarium played an

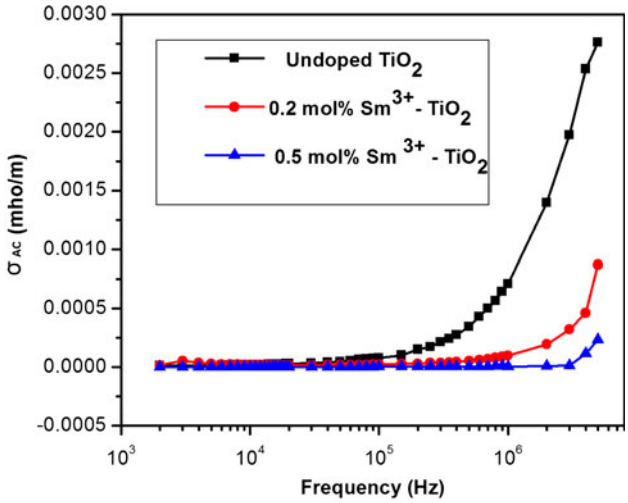

Fig. 8. Variation of AC conductivity with frequency of undoped TiO_2, 0.2 mol% Sm^{3+}-TiO_2, and 0.5 mol% Sm^{3+}-TiO_2 nanoparticles.

important role in the interfacial charge transfer.[5,23,24] Samarium ions could act as effective electron scavengers to trap the conduction-band electrons of TiO_2, hence the polarization effect decreased.

The AC conductivity (σ_{AC}) of the samples was calculated using the dielectric equation

$$\sigma_{AC} = \omega\varepsilon_0\varepsilon_r \tan\delta,$$

where ω is the angular frequency and ε_0 is the permittivity of free space. Figure 8 shows the variation of AC conductivity as a function of frequency for undoped and doped TiO_2 nanoparticles at room temperature. It was observed that, in all the samples, AC conductivity was constant up to 100 kHz and thereafter increased steeply as in the disordered materials. Also, at higher frequencies, the AC conductivity of undoped TiO_2 was reduced by Sm^{3+} doping. As the particle size decreased, the surface–volume ratio increased and large surface scattering occurred, which resulted in a reduction in the electronic conductivity.[25] The high conductivity at higher frequencies confirmed the polaron hopping in the synthesized sample. In the high frequency region, the short-range intrawell hopping of charge carriers between localized states occurred in a disordered manner.[26] However, in Sm^{3+}-doped TiO_2, Sm^{3+} ions effectively captured charge carriers, which in turn reduced the number of charge carriers which were intrawell hopping; hence conductivity was found to decrease.

CONCLUSIONS

Sm^{3+}-doped thermally stable titania nanoparticles (TiO_2) in the anatase phase were synthesized using a low-temperature hydrothermal method without any high-temperature calcination. XRD, BET surface area, SEM, and TEM analyses confirmed that the samarium doping resulted in the formation of anatase phase TiO_2 nanoparticles with an average particle size of 31 nm and a reduction of crystallite size to 12 nm and 10 nm. EDS spectra revealed the atomic percentages of Ti and Sm^{3+} in the synthesized samples. TG and DTA results showed the thermal stability of the materials over a wide temperature range. The TiO_2 nanoparticles had high dielectric constant and displayed an abrupt dielectric relaxation in the low frequency range. The presence of samarium ions significantly reduced the dielectric constant and AC conductivity. The loss tangent peak of TiO_2 nanoparticles that appeared at a characteristic frequency of 1 kHz was shifted to the higher frequency of 2 kHz on doping with Sm^{3+} ions. The peak intensity increased with the increase in the dopant concentration. Also a frequency-independent behavior was observed above 100 kHz for all the samples.

ACKNOWLEDGEMENTS

One of the authors, A.K.A.G., gratefully acknowledges the University Grants Commission, Government of India, for the award of a research fellowship under the Faculty Improvement Programme (FIP). The authors would like to thank Prof. Zoltan Racz, Eötvös University, Hungary for assistance with revising the manuscript.

REFERENCES

1. M.R. Hoffmann, S.T. Martin, W. Choi, and D.W. Bahnemann, *Chem. Rev.* 95, 69 (1995).
2. K. Shankar, J. Bandara, M. Paulose, H. Wletash, O.K. Varghese, G.K. More, M. Thelakkat, and C.A. Grimes, *Nanoletters* 8, 1654 (2008).
3. D. Kuang, J. Brillet, P. Chen, M. Takata, S. Uchida, H. Miura, K. Sumioka, S.M. Zakeeruddin, and M. Gratzel, *ACS Nano* 2, 1113 (2008).
4. S.W. Kim, T.H. Han, J. Kim, H. Gwon, H.S. Moon, S.W. Kang, S.O. Kim, and K. Kang, *ACS Nano* 3, 1085 (2009).
5. T. Jesty, K. P. Kumar, and M. Suresh, *Sci. Adv. Mater.* 2, 481 (2010).
6. S.K. Kim, W.D. Kim, K.M. Kim, C.S. Hwang, and J. Jeong, *Appl. Phys. Lett.* 85, 4112 (2004).
7. Z.R. Khan, D.C. Hasko, M.S.M. Saifullah, and M.E. Welland, *J. Phys: Condens. Matter* 21, 215902 (2009).
8. G.A. Battiston, R. Gerbasi, M. Porchia, and P. Marina, *Thin Solid Films* 239, 186 (1994).
9. C. Lee, P. Ghosez, and X. Gonze, *Phys. Rev. B* 50, 13379 (1994).
10. T. Trung, W.J. Cho, and C.S. Ha, *Mater. Lett.* 57, 2746 (2003).
11. C.H. Lu and M.C. Wen, *J. Alloys Compd.* 448, 153 (2008).
12. D. Byun, Y. Jin, B. Kim, J.K. Lee, and D. Park, *J. Hazard. Mater.* 73, 199 (2000).
13. E. Gyorgy, G. Socol, E. Axente, I.N. Mihailescu, C. Ducu, and S. Cluca, *Appl. Surf. Sci.* 247, 429 (2005).
14. B. Jiang, H. Yin, T. Jiang, J. Yan, Z. Fan, L. Changsheng, W. Jing, and Y. Wada, *Mater. Chem. Phys.* 92, 595 (2005).
15. Hengbo Yin, Yuji Wada, Takayuki Kitamura, Takayuki Sumida, Yasuchika Hasegawa, and Shozo Yanagida, *J. Mater.Chem* 12, 378 (2002).
16. H. Yin, Y. Wada, T. Kitamura, S. Kambe, S. Murasawa, H. Mori, T. Sakata, and S. Yanagida, *J. Mater. Chem.* 11, 1694 (2001).
17. K. Funke, *Prog. Solid State Chem.* 22, 111 (1993).
18. S. Mona and M.S.A. Abdel-Mottaleb, *Inorg. Chem. Acta* 360, 2863 (2007).
19. Q. Xiao, Z. Si, Z. Yu, and G. Quì, *J. Alloys Compd.* 450, 426 (2008).

20. S. Je-Lueng, L. Chia-Hsiang, C. Chyow-San, C. Chang-Tong, C. Chia-Chi, and C. Ching-Yuan, *J. Hazard. Mater.* 155, 164 (2008).
21. A. Kubacka, M. Ferrer, A. Marty'nez-Arias, and M. Fernández-García, *Appl. Catal. B* 84, 87 (2008).
22. Z. De, P. Tianyou, X. Jiangrong, Y. Chunhau, and K. Xuezhi, *Mater. Lett.* 61, 105 (2007).
23. J.M. Coronado, A.J. Maria, A. Martinez-Arias, J.C. Conesa, and J. Soria, *J. Photochem. Photobiol.* A150, 213 (2002).
24. Y.B. Xie and C.W. Yuan, *Appl. Catal. B* 46, 251 (2003).
25. K. Karthik, S. Kesavapandian, and N. VictorJaya, *Appl. Surf. Sci.* 256, 6829 (2010).
26. B. Kumar and G. Srivastava, *J. Appl. Phys.* 75, 6115 (1994).